Research Paper

Conversion of the hydrochar recovered after levulinic acid production into activated carbon adsorbents

Domenico Licursi [a,b,*], Claudia Antonetti [a,b], Nicola Di Fidio [a,b], Sara Fulignati [a,b], Patricia Benito [c], Monica Puccini [d], Sandra Vitolo [d], Anna Maria Raspolli Galletti [a,b]

[a] Dipartimento di Chimica e Chimica Industriale – Università di Pisa, Via Giuseppe Moruzzi 13, 56124 Pisa, Italy
[b] Consorzio Interuniversitario Reattività Chimica e Catalisi (CIRCC), Via Celso Ulpiani 27, 70126 Bari, Italy
[c] Dipartimento di Chimica Industriale "Toso Montanari", Alma Mater Studiorum – Università di Bologna, Viale Risorgimento 4, 40136 Bologna, Italy
[d] Dipartimento di Ingegneria Civile e Industriale – Università di Pisa, Largo Lucio Lazzarino, 56122 Pisa, Italy

ARTICLE INFO

ABSTRACT

Levulinic acid production by acid-catalyzed hydrothermal conversion of (ligno)cellulosic biomass generates significant amounts of carbonaceous hydrochar, which is currently considered a final waste. In this work, the hydrochar recovered after the levulinic acid production, was subjected to cascade pyrolysis and chemical activation treatments (by H_3PO_4 or KOH), to synthesize activated carbons. The pyrolysis post-treatment was already effective in improving the surface properties of the raw hydrochar (Specific Surface Area: 388 m^2/g, V_P: 0.22 cm^3/g, V_{MESO}: 0.07 cm^3/g, V_{MICRO}: 0.14 cm^3/g), by removing volatile compounds. KOH activation resulted as the most appropriate for further improving the surface properties of the pyrolyzed hydrochar, showing the best surface properties (Specific Surface Area: 1421 m^2/g, V_P: 0.63 cm^3/g, V_{MESO}: 0.10 cm^3/g, V_{MICRO}: 0.52 cm^3/g), which synergistically makes it a promising system towards adsorption of CO_2 (~90 mg/g) and methylene blue (~248 mg/g). In addition, promising surface properties can be achieved after direct chemical activation of the raw hazelnut shells, preferably by H_3PO_4 (Specific Surface Area: 1918 m^2/g, V_P: 1.34 cm^3/g, V_{MESO}: 0.82 cm^3/g, V_{MICRO}: 0.50 cm^3/g), but this choice is not the smartest, as it does not allow the valorization of the cellulose fraction to levulinic acid. Our approach paves the way for possible uses of these hydrochars originating from the levulinic acid chain for new environmental applications, thus smartly closing the biorefinery loop of the hazelnut shells.

1. Introduction

Hazelnut is the fifth most produced tree nut in the world, with an estimated production of about 545 thousand metric tons in 2022 (Statista, 2022), involving Turkey and Italy among the main world's leading producers. Because of its industrial processing, different waste streams are produced, above all shells, which represent approximately 50 wt% of the total nut (about 273 thousand metric tons, based on the 2021–2022 worldwide data) (Statista, 2022). Shells are mostly used for domestic heating and landscaping but can be more advantageously exploited for the recovery of added-value bio-products, such as oligosaccharides and phenolics (Rivas et al., 2020), or to produce bio-chemicals, such as levulinic acid (LA) (Licursi et al., 2017). LA is an industrially attractive platform chemical (precursor of fuel additives, fragrances, solvents, pharmaceuticals, and plasticizers) (Di Bucchianico et al., 2022), and its

industrial production has been optimized by GFBiochemicals (2023), in the perspective of using waste biomasses as starting feedstocks. A recent techno-economic analysis of the LA process has confirmed excellent water management, making it appropriate for the conversion of both wet and dry biomasses (Hurtado et al., 2021; Silva et al., 2018). LA synthesis requires the acid-catalyzed hydrothermal conversion of the cellulosic fraction of the biomass, effectively carried out in the presence of diluted mineral acids (HCl or H_2SO_4) and temperatures/times generally up to 200 °C/1h (Dutta et al., 2022a). Some modifications of the traditional approach have been proposed, including the use of different acid catalysts, as well as organic co-solvents, the latter employed to perform an organosolv delignification, thus improving the hydrolysis kinetics (Dutta et al., 2022a, 2022b). However, the traditional mineral-based hydrothermal approach remains the preferred choice for the industrialization of the LA process.

Hydrochar is always produced as the solid waste of the LA process, and it includes both the degraded lignin and the furanic by-products (humins), originating from the degradation reactions of C5/C6 carbohydrates (Wan et al., 2019). Because of the occurrence of such reactions, the resulting lignin residue chemically differs from the native one and, to better mark this difference, it is often called "pseudo-lignin" (Shinde et al., 2018). In general, the lignin fraction is almost insoluble in the acidic water medium, instead undergoing carbonization (Correa et al., 2017). Regarding the humin formation, it involves species such as α-carbonyl aldehydes (mainly 2,5-dioxo-6-hydroxyhexanal), occurring by hydrolytic ring-opening of soluble furanic intermediates (such as 5-hydroxymethylfurfural and furfural) (Shi et al., 2019). For lignin-rich feedstocks, such as the hazelnut shells herein of interest, and taking into account the high formation of humins under the conditions required for LA production, it becomes really important to exploit the hydrochar waste stream, as demonstrated by recent techno-economic analyses (Kumar et al., 2020). To identify new exploitation strategies of hydrochars, these are often compared with biochars, the latter traditionally obtained by pyrolysis (Tripathi and Sahu, 2016). Both hydrochars and biochars are exploitable as organic amendments for agricultural soils (Libra et al., 2011) and soil remediation (Zhang et al., 2020), suitably considering their physico-chemical differences. In this context, hydrochar has generally an acidic pH, prevailing aliphatic behavior and reduced immobilization towards heavy metals, whilst biochar is characterized by alkaline pH, prevailing aromatic texture and greater stabilization towards heavy metals (Cui et al., 2022; Gascó et al., 2018). The specific exploitation of the hydrochar for adsorption purposes is an attractive possibility also considering specific techno-economic evaluations of the LA process (Deng et al., 2022; Santana Junior et al., 2020). Unfortunately, the raw hydrochar shows very low specific surface area (SSA) and prevailing macroporosity, thus making necessary additional chemical and/or physical activation treatments, to markedly improve its surface properties. For this purpose, physical activation methods are often applied, mainly including traditional modifications with gases (steam, CO_2, ozone, and air) (Sajjadi et al., 2018). Instead, chemical activation requires char impregnation with chemical agents, such as neutral ($FeCl_3$, $ZnCl_2$, $CaCl_2$, $MgCl_2$, etc.), acidic (H_3PO_4, H_2SO_4, HNO_3, H_2O_2, etc.), alkaline (NaOH, KOH, K_2CO_3, Na_2CO_3, etc.), and self-activating (organic acid salts of Na, K, and Ca, such as citrate, oxalate, gluconate, acetate, etc.) ones (Gao et al., 2020). Chemical activation offers significant advantages over physical methods, producing activated carbons (ACs) with improved surface properties (Alcañiz-Monge et al., 2022; Romero-Anaya et al., 2014). The efficiency of the activation treatment is often confirmed by adsorbing appropriate probe molecules as benchmarks. In this context, CO_2 is proposed for gas–solid studies (Zubbri et al., 2021), whilst methylene blue (MB) is attractive for liquid–solid ones (Pandey et al., 2022). The application of char as a CO_2 adsorbent is industrially attractive, showing potential advantages, in terms of low cost, good availability and easy regeneration. Up to now, different biomass feedstocks (bamboo, giant reed, coconut shells, microalgae, lignin waste, chitosan, etc.) have been employed to synthesize such adsorbent materials, mainly by acid (H_3PO_4) or alkaline (KOH) activations, which destroy the fibrous cellular structure of the biomass, generating porous surfaces (Jibril et al., 2008). The claimed CO_2 uptakes fall within the range 2.0–6.0 mmol g^{-1} at low temperatures (0–50 °C) and pressures (≤ 1 bar), depending on the activation conditions (activating agent type and ratio, activation temperature, and time) (Sevilla et al., 2019). According to Sevilla and Fuertes (2011a), the CO_2

adsorption capacity of chars is strongly influenced by the pore size distribution and, more specifically, by the presence of narrow-size micropores (<1 nm). In the field of solid–liquid adsorption, MB removal from wastewater is receiving increasing interest. Remarkably, Santoso et al. (2020) have specifically reviewed the studies on the adsorption of this dye, classifying the available carbon-based materials based on the MB adsorption efficiency, respectively as superior (higher than 1000 mg/g), excellent (500–1000 mg/g), moderate (100–500 mg/g), and poor (<100 mg/g). In principle, both high surface area (>1000 m^2/g) and moderate pore diameter (up to 6 nm) positively act towards this adsorption process (Santoso et al., 2020), and chemical activation is generally required to improve such MB adsorption performances, especially in the case of the hydrochar (Güleç et al., 2022).

Despite all the discussed progresses in this field of research, only a few studies report the complete exploitation of each biomass component. After having optimized the LA production from hazelnut shells (Licursi et al., 2017), in this work, the conversion of the corresponding hydrochar into a new cheap adsorbent, was investigated. For this purpose, a pyrolysis post-treatment and chemical activation treatments (H_3PO_4 and KOH) of this hydrochar were considered, in a cascade approach. The characterization of the synthesized ACs was carried out, to identify the most promising ACs, to be used for the gas–solid and liquid–solid adsorption tests, with carbon dioxide and MB as the probe molecules, respectively. The proposed integrated approach makes it possible to fully exploit the hazelnut shell feedstock, smartly closing the biorefinery cycle of the hazelnut wastes, according to a sustainable and circular perspective.

2. Materials and methods

2.1. Chemical composition of the raw biomass

Hazelnut shells of *Tonda Gentile Romana* variety were provided by Stelliferi-Itavex S.p.A., Caprarola, Viterbo (VT), Italy. According to our previous work (Licursi et al., 2017), the corresponding chemical composition is the following (on a dry matter): cellulose (22.9 wt%), hemicellulose (23.5 wt%), Klason lignin (37.6 wt%), uronic acids (5.0 wt%), ash (1.4 wt%), ethanol-extractives (1.4 wt%), and others (8.2 wt%).

2.2. Hydrochar production

Raw hydrochar was produced according to the acid-catalyzed hydrothermal treatment of the same feedstock (Licursi et al., 2017). Briefly, a 600 mL Parr zirconium-made autoclave, controlled through a Parr controller 4848, was used for the hydrochar production, employing the formulation and the best reaction conditions identified for LA synthesis: biomass (24.5 g), water (350 g), and HCl 37 wt% (17.8 g), working at 180 °C for 180 min, under autogenous pressure.

2.3. Hydrochar pyrolysis

Raw hydrochar was pyrolyzed in a Lenton LTF 12/25/250 tubular oven. For this purpose, the dried sample was weighed in a ceramic boat, then transferred inside the furnace, and heated up to 600 °C, under a constant N_2 flow of 500 mL/min, with a heating rate of 10 °C/min. The yield in the pyrolyzed hydrochar was calculated as follows:

$$Yield\ in\ pyrolyzed\ hydrochar\ (wt\%) = \frac{dried\ solid\ residue\ recovered\ after\ pyrolysis\ (g)}{dried\ biomass\ before\ pyrolysis\ (g)}$$

2.4. Chemical activation of the raw biomass and pyrolyzed hydrochar

Different chemical activation procedures (H_3PO_4 and KOH) were performed on the raw biomass and pyrolyzed hydrochar. In this context, direct chemical activation of the raw biomass was carried out as a benchmark for that of the pyrolyzed hydrochar, the latter resulting of greater interest for our purpose. Regarding the acid activation (H_3PO_4), an acid/precursor ratio of 3.7:1 wt/wt was employed on the raw biomass, whilst 1:1 wt/wt on the pyrolyzed hydrochar, according to the experimental procedures provided by Rao Ganga et al. (2016) and Suárez-García et al. (2002), respectively. Besides the acid/precursor ratio, the two procedures differ in the adopted activation temperatures/ times, equal to 400 °C/2h and 500 °C/1 h, for the raw biomass and the pyrolyzed hydrochar, respectively. Instead, KOH activation was carried out by physical mixing of the activating agent/precursor ratio of 4:1 wt/ wt, according to the experimental procedure described by Sevilla et al. (2011b).

After each activation treatment, the AC yield was calculated as:

$$AC\,yield\,(wt\%) = \frac{Recovered\,AC\,(g)}{Starting\,precursor\,(g)} \times 100 \qquad (2)$$

2.5. Elemental analysis

Samples were characterized by elemental analysis for the quantification of C, H, N, and O content, by using an automatic analyzer LECO TruSpec. C and H contents were determined by an infrared spectroscopy detector, whilst N content was determined by a thermal conductivity detector. Lastly, O content was determined by difference: O (%) = 100 (%) − C (%) − H (%) – N (%) – Ash (%).

2.6. Proximate analysis

Proximate analysis was carried out by using a thermogravimetric balance Q500 TA INSTRUMENTS. 12 ± 1 mg of sample were weighed and heated for the determination of moisture and volatile matter, by adopting the following program: from 30 to 900 °C heating at 20 °C/ min, under N_2 flow (100% v/v). Then, the sample was cooled down from 900 to 800 °C, under a flow of [nitrogen (40% v/v)–air (60% v/v)], for the determination of fixed carbon and ash.

2.7. FT-IR analysis

FT-IR (Fourier Transform-Infrared Spectroscopy) analysis was performed by a Perkin Elmer "Spectrum-Two" spectrophotometer. IR spectra were acquired by the KBr pellet technique, maintaining the same sample concentration (1.5 mg of sample + 180 mg of KBr) and thickness of each pellet (200 ± 10 μm). The acquisition of each spectrum required 12 scans, with a resolution of 8 cm^{-1}, and the acquired spectra were normalized to 100 % of transmittance.

2.8. Energetic properties

The higher heating value (HHV) of the pyrolyzed hydrochar was determined according to the UNIEN 15400:2011 procedure, by using a home-built isoperibol calorimeter, equipped with a standard Berthelot-Mahler calorimetric bomb, whose inner volume was about 400 cm^3. Further details are reported in our previous work (Licursi et al., 2017). Based on the acquired HHV data, the energy densification ratio was calculated as follows:

$$Energy\,densification\,ratio = \frac{HHV\,of\,dried\,product}{HHV\,of\,dried\,raw\,biomass} \qquad (3)$$

2.9. Single-Point determination of SSA (SP-SSA)

A ThermoQuest Surface Area Analyzer Qsurf S1 was used for the determination of SP-SSA of the ACs synthesized from raw biomass and pyrolyzed hydrochar. Before the measurement, the sample was treated at 130 °C for 12 h under a nitrogen flow of 35 mL/min. Subsequently, the sample was cooled down to the temperature of the liquid nitrogen (77 K) for the measurement.

2.10. Multi-Point determination of SSA (MP-SSA), pore volume and size distribution

Determinations of MP-SSA, pore-volume, and size distribution of the ACs were carried out using a Micromeritics ASAP 2020 instrument by N_2 adsorption/desorption at −196 °C. Before the analysis, the samples were degassed under vacuum, and heated to 110 °C for 240 min. at a pressure below 15 μmHg. MP-SSAs were calculated using the Brunauer-Emmet-Teller (BET) method. Total pore volumes were calculated at p/p^0 = 0.995. The t-plot was used to calculate the micropore area and volume and the external surface area. The mesopores were investigated by the Barret-Joiner-Halenda (BJH) method in the adsorption branch. Micropore size distributions were obtained by NLDFT. Powders in the form of ground and 600 mm sieved samples were analyzed.

2.11. SEM analysis

Micrographs were acquired by SEM electron microscope (Jeol JSM5600LV). The sample was previously metalized with a gold molecular film, using the Edwards Sputter Coater metallizer.

2.12. Gas-phase adsorption of CO_2

A Q500 TA INSTRUMENTS thermogravimetric balance was used for the gas-phase adsorption of CO_2. The sample (12 ± 1 mg) was weighed in a platinum crucible and directly conditioned in the thermobalance, with a constant flow of N_2 (100 mL/min), then it was heated according to the following temperature ramp: from room temperature to 105 °C with a heating rate of 20 °C/min, then held for 10 min at this temperature and then cooling down to room temperature. Then, the sample was ready to undergo CO_2 adsorption, which was realized by flowing 100 mL/min of a CO_2/N_2 gas mixture (CO_2 60 %v/v + N_2 40 %v/v), at 27 °C and atmospheric pressure. When the equilibrium was reached, the desorption was carried out by switching the gas flow to 100 %v/v N_2. The adsorption curves show the uptake in sample weight (mg/g) as a function of the time (min).

2.13. Liquid-solid adsorption of MB

100 or 10 mg of the sample were added to 25 mL of a solution 0.1 g/L of MB, monitoring the adsorption kinetics up to the equilibrium conditions. A small amount of liquid was sampled at different times, then it was centrifuged and filtered. For the quantitative determination of the adsorbed MB, a Jasco UV–Vis spectrophotometer was used, acquiring the absorbance of the sample at 657 nm, after appropriate dilution. The quantitative determination of the MB was performed by the external standard method, thus acquiring the absorbance of solutions of known concentration (0.001–0.0066 g/L) of MB. The amount of adsorbed MB at time t (q_t, in mg/g), was obtained through the mass balance (4):

$$q_t = \frac{(C_0 - C_t)V}{m} \qquad (4)$$

where C_0 and C_t are the concentrations (in mg/L) of the MB solution at the beginning and at the sampling time, V is the volume of the sampled solution (L), and m is the mass of the sample (g). The data were processed according to the pseudo-second-order model, according to the following equations:

$$\frac{dq}{dt} = k_2(q_e - q_t)^2 \tag{5}$$

$$\frac{t}{q_t} = \frac{1}{k_2 q_e^2} + \frac{1}{q_e} t \tag{6}$$

where k_2 (in g/mg·min) is the pseudo-second-order constant, q_t (in mg/g) is the mass of adsorbed solute per gram of sample at time t and q_e (mg/g) is the maximum amount of adsorbed solute at the equilibrium. The adsorption constant k_2 was obtained from the intercept of the above-linearized equation, after the calculation of q_e as the slope. The MB adsorption was expressed as follows:

$$AdsorbedBM = \frac{RemovedMB(mg)}{AC(g)} \tag{7}$$

On this basis, MB removal efficiency (η%) was calculated, as follows:

$$\eta\% = \frac{Amount\,of\,adsorbed\,MB(mg)}{Amound\,of\,starting\,MB(mg)} x100 \tag{8}$$

3. Results and discussion

3.1. Modification of the raw hydrochar surface properties by slow-pyrolysis post-treatment

To improve the surface properties and aromaticity of the raw hydrochar (Bahcivanji et al., 2020), which was previously synthesized by us in high yield (45 wt%) within the LA production chain (Licursi et al., 2017), now different slow-pyrolysis tests were performed, working in a tubular furnace (heating rate = 10 °C/min, N2 flow = 500 mL/min) at different temperatures (in the range 400–700 °C). Under the adopted reaction conditions, SP-SSA reached a maximum of about 360 m^2/g at 600 °C, obtaining a corresponding yield in pyrolyzed hydrochar of about 50–55 wt%, calculated with respect to the weight of the starting raw hydrochar. FT-IR analysis of the best-pyrolyzed hydrochar was carried out, to confirm the occurred devolatilization (see Supplementary material). FT-IR spectrum of pyrolyzed hydrochar reveals a decrease in the band intensities due to the stretching of O–H (3000–3500 cm^{-1}) and C–H (2935 cm^{-1}) bonds (Licursi et al., 2017), which suggests a decrease in polar functional groups. The absorption band at about 1740 cm^{-1} in the raw biomass (C = O stretching vibrations of esters) is shifted at 1700 cm^{-1} in the raw hydrochar (C = O stretching vibrations of carboxylic acids, ketones, and aldehydes), and this latter is significantly decreased in the pyrolyzed hydrochar, confirming the devolatilization of trapped organic compounds (such as LA and formic acid) (Licursi et al., 2017). The intense absorption band at about 1600 cm^{-1} present in all samples is assigned to C = C stretching and skeletal vibrations of aromatic rings (Licursi et al., 2017), and becomes more intense going from the raw biomass to the raw and pyrolyzed hydrochar, thus confirming the carbonization advance. The absorption bands between 1300 and 900 cm^{-1} are assigned to C-O stretching vibrations of oxygenated functionalities (Licursi et al., 2017) and become less evident going from the raw biomass to the raw and pyrolyzed hydrochar, demonstrating that deoxygenation has taken place. Furthermore, the appearance of intense absorption bands in the pyrolyzed hydrochar within the region 900–750 cm^{-1}, due to bending vibrations of the aromatic = CH2 and CH bonds, confirms the occurred dehydration/condensation among the aromatic domains (Falco et al., 2011). Such a char aromatization reduces the risk of leaching phenomena (phytotoxicity), which is a highly desirable property for soil amendment uses (Bahcivanji et al., 2020), and soil remediation purposes (Cui et al., 2022; Wang et al., 2019). The modification of hydrochar surface properties for the synthesis of ACs and its integration within the main LA supply chain is well-supported by very recent techno-economic analyses (Chaparro-Garnica et al., 2022). These indicate that this exploitation possibility is interesting to be further investigated and developed. Considering the LA process, at least a two-stage carbonization of the hazelnut shells is necessary for ACs synthesis

(e.g. hydrothermal carbonization of hazelnut shells for LA production + physical or chemical post-activation of the resulting hydrochar). Besides, if compared with the direct activation of raw biomass (e.g. one-stage chemical activation), the two-stage approach can improve both the final yield in stable carbon and the corresponding surface properties (Alcañiz-Monge et al., 2022; Bahcivanji et al., 2020). Remarkably, also the two-stage pyrolysis (e.g. biomass pyrolysis + cascade chemical activation of the pyrolyzed biochar) has been proposed for improving the yield and textural properties of biochars originating from agricultural wastes (Zubrik et al., 2017). Although the pyrolysis treatment is energetically more demanding than the hydrothermal one, such thermal treatments are still economically interesting, if char is exploited for the synthesis of much high added-value adsorbents.

Remarkably, HHV of the pyrolyzed hydrochar was 27.4 MJ/kg, while the value for the raw hydrochar was 24.7 MJ/Kg (Licursi et al., 2017). The increased value is mainly ascribed to the removal of oxygenated compounds and to the progress of carbonization. Moreover, considering that HHV of the raw biomass was 18.8 MJ/Kg (Licursi et al., 2017), the energy densification ratio of the pyrolyzed hydrochar increased to 1.5 (versus 1.3 of the raw hydrochar).

3.2. Synthesis and characterization of ACs: Results

After the pyrolysis post-treatment, a chemical activation was carried out on the pyrolyzed hydrochar, to deeply modify its surface properties. To the best of our knowledge, an overall three-stage treatment has been proposed only by Tran et al. (2017) on the golden shower (*Cassia Fistula*) biomass, resulting effective for progressively improving the carbon stability and the corresponding surface properties. In our case, chemical activation of the pyrolyzed hydrochar was carried out with H3PO4 and KOH, and the same activation treatments were done on the raw biomass, as a benchmark. The impregnation ratio is one of the main parameters to improve the surface properties of the char, generally within the range of 1–4 wt/wt (Delgado and Mendez, 2014). High impregnation ratios are desired for improving the SSA and the total pore volume, unfortunately at the expense of the AC yield (Delgado and Mendez, 2014). Therefore, before proceeding with the in-depth characterization of the synthesized ACs, it is of paramount importance to find a balanced compromise between AC yield and SSA, selecting the most interesting ACs, to be characterized more in-depth and tested for adsorption purposes. On this basis, different activation tests were carried out, aimed at maximizing both the yield and SP-SSA of the ACs. The best results obtained for ACs synthesized from raw biomass and pyrolyzed hydrochar are shown in Fig. 1:

The activation with H3PO4 gives the highest AC yield, starting from both types of precursors. However, this activation procedure leads to
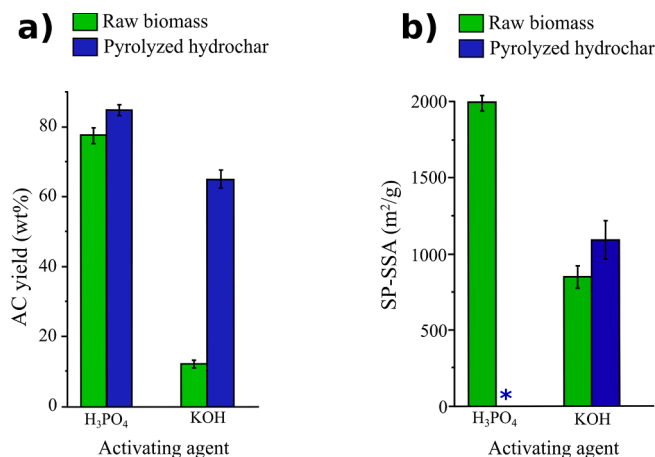

Fig. 1. (a) Yield (wt%) and (b) SP-SSA (m^2/g) of the synthesized ACs. Note *: negligible SP-SSA.

high SP-SSAs only in the case of the raw biomass, because H_3PO_4 mildly acts on dehydration/solubilization of the carbohydrates. Remarkably, in this case, the AC yield is high (~78 wt%), considering that this yield is directly evaluated with respect to the weight of the starting biomass. However, in this way, the preliminary exploitation of the cellulose fraction (e.g. the LA synthesis) has not been pursued, thus achieving only a limited exploitation of the biomass components. SP-SSA is negligible in the case of the pyrolyzed hydrochar - H_3PO_4 AC, due to the acid-catalyzed condensation reactions occurring among humins and/or lignin, and/or other reactive compounds. In this context, it is known that humin formation is favored under acidic conditions (Björnerbäck and Hedin, 2019), such as those highly required for LA synthesis (in this work considered as upstream biomass processing). Moreover, this growth continues over time, thus causing their continuous precipitation, because of the molecular weight increase (Cheng et al., 2020). On this basis, acid activation of pyrolyzed hydrochar is not appropriate for our purpose, instead enabling further aggregation of humins, which leads to unsatisfactory SP-SSAs of the corresponding AC (Wang et al., 2011). On the other hand, alkaline activation of the pyrolyzed hydrochar resulted particularly effective, leading to higher SP-SSAs. An alkaline environment is effective for the removal of residual organic compounds, such as humins (van Zandvoort et al., 2015), avoiding the above issues related to acid activation. SP-SSAs obtained after KOH activation of the raw biomass and pyrolyzed hydrochar are similar. Remarkably, these values are higher than those reported by Kabakcı and Baran (2019), who activated with KOH different hydrochars deriving from lignocellulosic biomasses, such as wood sawdust, olive pomace, walnut shell, apricot seed, tea stalk, hazelnut husk (KOH/hydrochar ratio = 2 wt/wt and SSAs within the range 308.9–666.7 m^2/g). The yield in the pyrolyzed hydrochar - KOH AC is high (e.g. amounting to ~ 65 wt%, evaluated with respect to the weight of the starting pyrolyzed hydrochar). Considering that, in the proposed three-stage activation procedure, intermediate pyrolysis and an upstream hydrothermal treatment have been additionally carried out, an overall AC yield of about 16 wt%, calculated with respect to the weight of the raw biomass, was achieved. This yield is lower than that obtained from the H_3PO_4 activation treatment of the raw biomass, however, the proposed strategy ensures better exploitation of the biomass fractions. Remarkably, the LA production already repays the economy of the process, and further exploitation of the hydrochar generates more economic surplus, which is undoubtedly much high for ACs, considered niche products. This preliminary screening has evidenced that the most valuable ACs, that could be advantageously used for the development of adsorption applications, are i) pyrolyzed hydrochar - KOH AC, and ii) raw biomass - H_3PO_4 AC. The characterization of these ACs has been carried out, to specifically select those of greatest interest for adsorption purposes. The results of the ultimate analysis are reported as Supplementary material. Pyrolyzed

hydrochar shows the highest C content and the lowest O and H content, mainly due to the removal of oxygenated volatile species, because of the pyrolysis treatment. Instead, ACs of interest have a slightly lower C content than pyrolyzed hydrochar, whilst O content is appreciably higher, which is indicative of the presence of additional oxygenated functionalities. Ultimate analysis data are advantageously reprocessed as H/C and O/C molar ratios, and plotted within a Van Krevelen diagram (Fig. 2):

H/C and O/C molar ratios allow following the evolution of the carbonization process, which occurs mainly through dehydration, progressively moving from the raw biomass (H/C = 1.36; O/C = 0.61) to the raw hydrochar (H/C = 0.80; O/C = 0.31) and pyrolyzed hydrochar (H/C = 0.52; O/C = 0.13). The low H/C and O/C molar ratios of the synthesized ACs confirm the carbonization progress, which occurred by dehydration/demethylation paths. Best carbonization performances have been achieved by KOH activation of the raw biomass (H/C = 0.14; O/C = 0.14) and the pyrolyzed hydrochar (H/C = 0.14; O/C = 0.18), highlighting their similarity. Somewhat higher ratios of the raw biomass - H_3PO_4 AC (H/C = 0.39; O/C = 0.28) and pyrolyzed hydrochar - H_3PO_4 AC (H/C = 0.38; O/C = 0.25) are indicative of more limited carbonization than that achieved by alkaline activation.

Proximate analysis of the pyrolyzed hydrochar and synthesized ACs was performed by thermogravimetric analysis, and the corresponding results are shown in Table 1, together with those of the raw biomass/hydrochar (Licursi et al., 2017):

The higher fixed C contents of the synthesized ACs confirm the occurred carbonization of the precursors and the degradation of the lighter organic matter (it is noteworthy the high fixed carbon content of pyrolyzed hydrochar). The decrease of the ash content, moving from raw biomass to raw hydrochar, indicates a partial solubilization of the inorganic components, resulting particularly effective working with hydrochloric acid, as in our hydrothermal LA process (Licursi et al., 2017). This is a desirable aspect, improving the corresponding physicochemical and fuel properties (Liu et al., 2019), and even better

Table 1

Proximate analysis of ACs, and comparison with raw biomass, raw hydrochar and pyrolyzed hydrochar.

Sample	Volatiles (%)	Fixed C (%)	Ash (%)
Raw biomass	76.1	22.4	1.6
Raw hydrochar	53.7	45.5	0.8
Pyrolyzed hydrochar	18.2	81.2	0.6
Raw biomass - KOH AC	22.8	68.0	9.1
Raw biomass - H_3PO_4 AC	26.2	69.7	4.1
Pyrolyzed hydrochar - KOH AC	24.5	69.4	6.1
Pyrolyzed hydrochar - H_3PO_4 AC	26.6	71.5	1.9
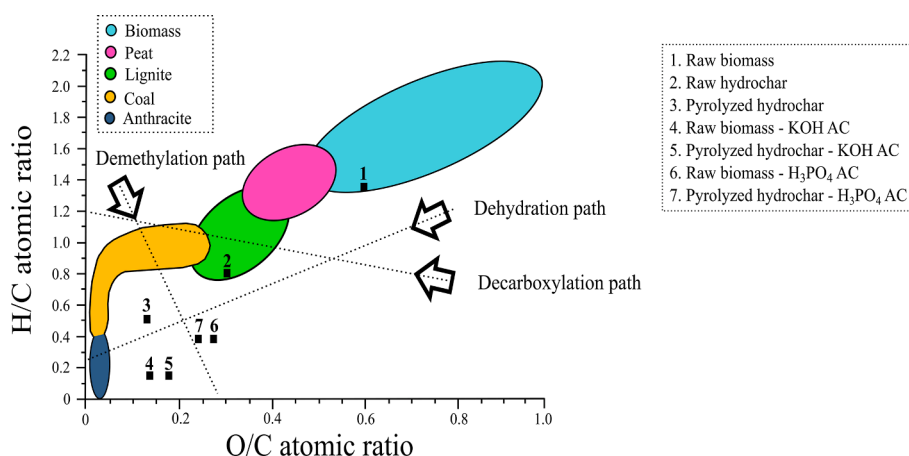
Fig. 2. H/C and O/C molar ratios (Van Krevelen diagram) of the ACs and comparison with raw biomass, raw hydrochar and pyrolyzed hydrochar.

exploitable for biomasses with a high ash content (He et al., 2022). Data reported in Table 1 highlight the higher content of ashes for the ACs, rather than for their precursors. In principle, high ash content is undesirable for the AC, resulting disadvantageous for its mechanical and surface properties. In this context, ashes tend to move freely on the AC surface, potentially limiting its available surface area, and covering its pores (especially micropores), which are unfavorable aspects for the development of such adsorption applications. In our investigation, both pyrolyzed hydrochar and synthesized ACs (Table 1) fully meet the minimum ash quality standards for commercial ACs, fixed at a maximum of 10 wt% (Zulkania et al., 2018). Moreover, as a further criterion for the quality acceptability of an AC, a minimum fixed carbon content of 65 wt%, is desirable (Zulkania et al., 2018). From this perspective, pyrolyzed hydrochar and all synthesized ACs fully meet these quality requirements, thus justifying the continuation of the study. On the other hand, raw hydrochar shows a too-low fixed-carbon content, requiring further processing (e.g. pyrolysis post-treatment) for improving its carbon stability, as previously stated.

Regarding the FT-IR analysis of the above ACs (see Supplementary material), in the spectra of KOH ACs, the absorption band at about 3400 cm^{-1} is assigned to O–H bond stretching vibration (Chen et al., 2014). Moreover, the absorption band in the range 1500–1600 cm^{-1} is ascribed to $C = C$ aromatic ring stretching vibrations, whilst that at around 1100–1200 cm^{-1} to C–O stretching vibrations (carboxylic acids, alcohols, phenols, ethers) (Chen et al., 2014). Regarding the H_3PO_4 AC, the absorption band at 3400 cm^{-1} is assigned to stretching vibrations of the hydroxyl groups deriving from adsorbed carboxyls, phenols, or alcohols, and water, whilst that between 1600 and 1400 cm^{-1} to $C = C$ stretching vibrations of aromatic units (Xu et al., 2014). The band centered at about 1190 cm^{-1} is due to C-O stretching vibrations in acids, alcohols, phenols, ethers, and/or esters groups, but also to C-O vibrations of C-O-P bonds and stretching mode of hydrogen-bonded $P = OOH$ groups from phosphates or polyphosphates (Xu et al., 2014). FT-IR spectra of the synthesized ACs confirm the structural modification of their precursors, e.g. their partial oxidation, defined by the prevailing presence of oxygenated functionalities.

N_2 adsorption/desorption isotherms at −196 °C of the ACs and their precursors were acquired (Supplementary material), thus determining the MP-SSA, total volume of pores (V_P), mesopores (V_{MESO}), micropores (V_{MICRO}), surface area of the micropores (A_{mic}), and the external surface area (A_{ext}). The acquired data are summarized in Table 2.

N_2 isotherm of the raw hydrochar is characteristic of non-porous or macroporous solids (Type II), whilst the small hysteresis loop can be related to interparticle pores. The isotherm is typical of hydrochars,

however, the N_2 adsorption capacity and, in turn, the MP-SSA, depend on the biomass precursor and the adopted hydrothermal conditions. Herein, MP-SSA of the raw hydrochar is 11 m^2/g, which is lower than the value of 30 m^2/g for the hydrochar from HTC of hazelnut shells (250 °C for 7.5 h), reported by Unur (2013). Only a very small quantity of pores in the mesopore range is identified in the pore size distribution (PSD) obtained by the BJH method. The non-porous profile of the sample is due to the presence of trapped compounds (Unur, 2013). The pyrolysis post-treatment has largely modified the surface properties of the raw hydrochar, leading to a significant improvement of the MP-SSAs, which is assessed to the prevailing contribution of the lignin texture, rather than to globular humins (Wortmann et al., 2022). Pyrolysis post-treatment has favored the development of a good microporosity, whose contribution amounts to 62.7% of the total pore volume, with the remaining volume contribution still due to mesopores. This porosity distribution, highly desired for our purposes, differs from that reported by Bahcivanji et al. (2020), who claimed a prevailing contribution of macro- and *meso*-porosity (>95%) for all their pyrolyzed hydrochars. This remarkable difference can be due to textural differences of the biomass feedstock (waste from parks and gardens), as well as to the different reaction conditions adopted for the hydrothermal carbonization (hydrothermal carbonization, instead of acid-catalyzed hydrothermal conversion to LA, as adopted in our approach) and/or for the pyrolysis post-treatment (longer reaction times than ours). The N_2 adsorption/desorption of the pyrolyzed hydrochar is a combination of Type I and Type II isotherms from the IUPAC classification. Most of the N_2 adsorption occurs at low relative pressures in micropores, and a plateau is then reached; the small N_2 uptake observed at p/p^0 close to 1 is related to the presence of some macropores. The hysteresis loop indicates the presence of interparticle pores. However, the micropores with diameters around 6Å represent the main contribution to the surface area (347 m^2/g A_{mic} vs 41 m^2/g A_{ext}) and pore volume (0.138 cm^3/g V_{mic} vs 0.075 cm^3/g V_{meso}).

The three-fold MP-SSA increase for the pyrolyzed hydrochar - KOH AC (1421 m^2/g) is related to the further development of microporosity (A_{mic}: 1359 m^2/g). The N_2 adsorption at very low relative pressures largely increased, while the contribution of the macropores remains almost unaltered. Remarkably, the pyrolyzed hydrochar - KOH AC, besides showing a high MP-SSA, is made by uniformly sized micropores with diameters at about 6 Å, providing a high micropore volume (0.5232 cm^3/g). It has been reported that KOH activation on pyrolyzed carbonaceous precursors from pits of olives and peaches (Molina-Sabio and Rodrìguez-Reinoso, 2004) and hydrothermal carbons (from glucose, cellulose and rye straw) also leads to a large development of the microporosity (Kabakcı and Baran, 2019). The development of a narrow micropore size distribution is also observed after direct activation of the raw biomass with KOH, as previously observed by Rechnia et al. (2012) for the activation of hazelnut shells by KOH. However, the micropore area (721 m^2/g) and volume (0.285 g/cm^3) are largely decreased. On the other hand, direct activation of the raw material with H_3PO_4 can develop both micro- and *meso*-pores (Molina-Sabio and Rodrìguez-Reinoso, 2004). The adsorption isotherm resembles both Type I and Type IV isotherms. The N_2 adsorption at low pressures is attributable to the presence of micropores; however, the "knee" of the adsorption curve is wider. While the continuous adsorption at increasing pressures is due to the filling of mesopores. The presence of a hysteresis loop may indicate well-formed mesopores. This sample shows the largest MP-SSA (1918 m^2/g), with a high contribution of both micro- (1107 m^2/g) and external-surface area (811 m^2/g), the latter can be related to mesopores. A bimodal distribution with wide micropores in the 4 to 15 Å range and mesopores between 20 and 100 Å is observed. An overall evaluation of the experimental data shows that the contribution of the micropores, in terms of percentages of the corresponding volumes, increases in the following order: raw biomass - H_3PO_4 AC (38 %) < pyrolyzed hydrochar (63 %) < raw biomass - KOH AC (71 %) < pyrolyzed hydrochar - KOH AC (83 %). Certainly, the activating agent has a key

Table 2

Apparent surface area (MP-SSA), total volume of pores (V_P), mesopores (V_{MESO}), micropores (V_{MICRO}), external surface area (A_{ext}) and surface area of micropores (A_{mic}) of the ACs and comparison with raw biomass, raw hydrochar and pyrolyzed hydrochar.

Sample	MP-SSA (m^2/g)	V_P (cm^3/g)	A_{mic} (m^2/g)	A_{ext} (m^2/g)	V_{MESO} (cm^3/g)	V_{MICRO} (cm^3/g)
Raw biomass	–	–	–	–	–	–
Raw hydrochar	11	0.066	–	–	0.066	–
Pyrolyzed hydrochar	388	0.220	347	41	0.075	0.138
Raw biomass - KOH AC	815	0.401	721	93	0.110	0.285
Raw biomass - H_3PO_4 AC	1918	1.337	1107	811	0.821	0.505
Pyrolyzed hydrochar - KOH AC	1421	0.629	1359	62	0.104	0.523
Pyrolyzed hydrochar - H_3PO_4 AC	2	–	–	–	–	–

role in the development of certain types of porosities, whereas H_3PO_4 is more favorable to the development of mesoporosity, whilst KOH to that of microporosity (e.g. compare the data related to raw biomass - H_3PO_4 and - KOH ACs). Instead, working with the same activating agent (KOH), the micropore contribution increases with the stage number of the chemical activation process, highlighting a better development of microporosity with our proposed three-step cascade activation (e.g. compare the data related to raw biomass-activated with KOH, pyrolyzed hydrochar and pyrolyzed hydrochar - KOH AC). This behavior is different than that observed by Tran et al. (2017), for a similar three-step activation on the golden shower (*Cassia Fistula*) biomass, whereas the non-micropore volume increased with the stage number of the chemical activation process, employing K_2CO_3 as (neutral) activating agent. This difference, related to the prevalence of mesopores over micropores, is always attributable to K_2CO_3, which is a much milder activating agent than KOH, such as H_3PO_4 (Yue et al., 2018). Therefore, the proposed three-step activation approach amplifies some surface properties of the activated carbon, e.g. developing a better prevalence of certain porosities, initially conferred by the type of activating agent. SEM microscopy helps monitor the carbonization progress, which occurred as a consequence of the different chemical treatments (Fig. 3).

SEM image of the raw biomass shows a compact but irregular texture, related to its high lignin content (Licursi et al., 2017). Instead, SEM analysis of the raw hydrochar reveals the presence of some spherical particles of pseudo-lignin source (Wan et al., 2019), whilst

pyrolyzed hydrochar shows a porous and accessible texture (Unur, 2013). The morphology of the synthesized ACs significantly differs from that of the corresponding precursors, due to the severity of the chemical activation treatments. Raw biomass - H_3PO_4 and - KOH ACs reveal their porous structure already at low magnification (1,000 x), whilst this is not appreciable for the pyrolyzed hydrochar - KOH AC with the same magnification. In this case, much higher magnifications are required (10,000 x) to visualize its porosity, and this AC appears much finer, because KOH has favored the development of microporosity, whilst H_3PO_4 activation has led to the prevailing development of mesoporosity, as previously stated. Lastly, the SEM image of the pyrolyzed hydrochar - H_3PO_4 AC confirms the absence of any significant accessible porosity, instead highlighting a flaked texture and the presence of globular humins, in agreement with the previous discussion on the poor surface properties of this AC.

3.3. Solid/gas adsorption of CO_2

Carbon capture and storage has been recognized as the most promising method for CO_2 control, so the use of such carbonaceous materials for CO_2 adsorption is highly attractive (Goel, 2021). After having evaluated the surface properties of the synthesized ACs, these were tested as CO_2 adsorbents at low CO_2 partial pressure (<1 bar), which is a typical condition provided for post-combustion capture at large power plants. Low adsorption temperature (room temperature) and a CO_2 partial
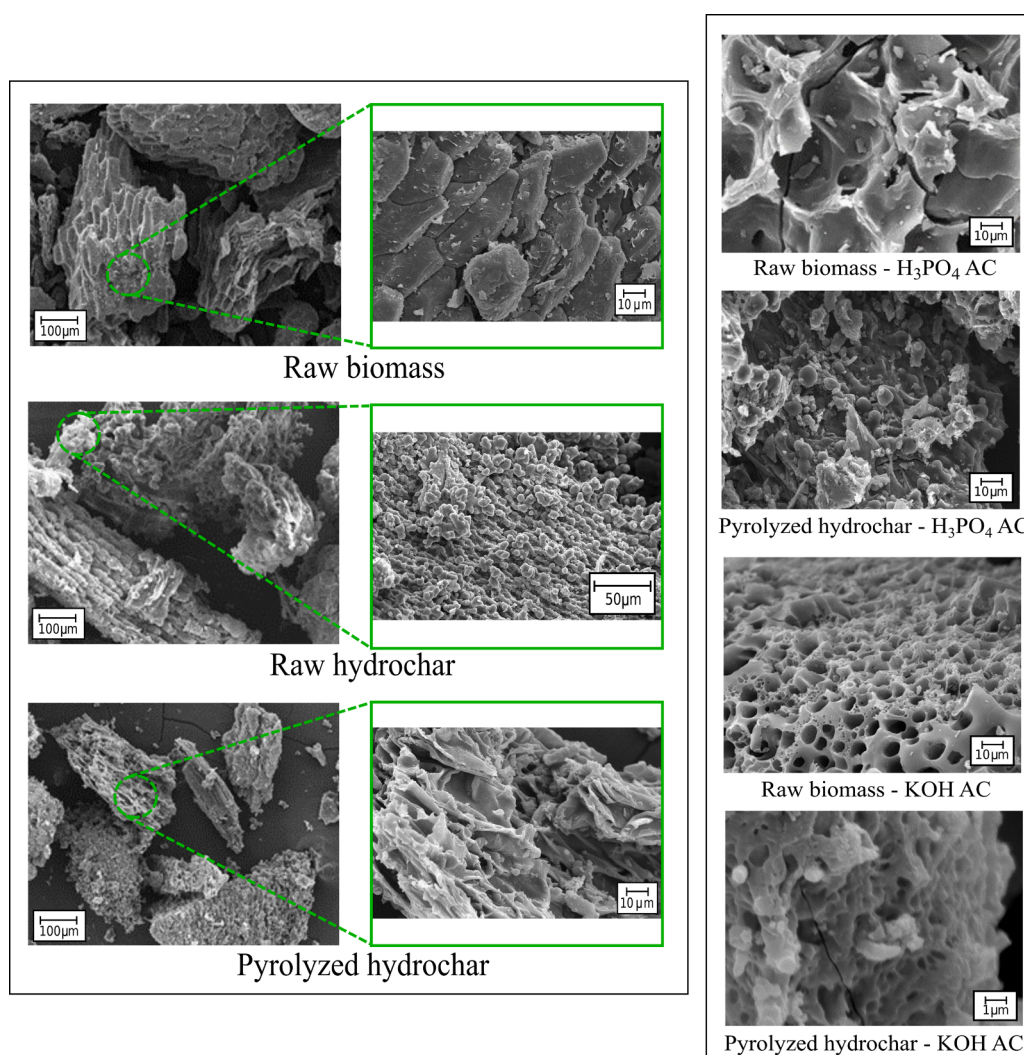

Fig. 3. SEM micrographs of ACs, and comparison with raw biomass, raw hydrochar and pyrolyzed hydrochar.
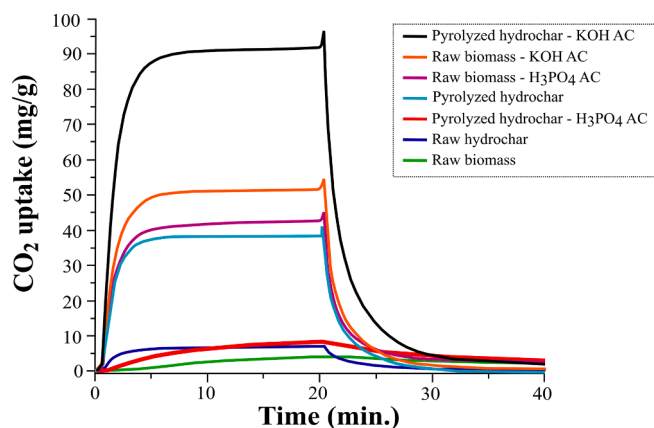
Fig. 4. CO_2 adsorption/desorption curves of ACs, and comparison with raw biomass, raw hydrochar and pyrolyzed hydrochar.

pressure of 0.60 bar (gas stream composition: 60 %v/v CO_2 + 40%v/v N_2) were adopted for the measurements. The adsorption/desorption curves of the synthesized ACs are reported in Fig. 4, showing the CO_2 uptake per gram of adsorbent (mg/g) as a function of the time (min). Here, the adsorption/desorption curves of the raw biomass and hydrochar are also reported, for comparison purposes.

The CO_2 adsorption/desorption curves of the raw biomass and raw hydrochar confirm, in both cases, poor performances towards CO_2 adsorption, in agreement with their almost negligible surface properties (Table 2). Pyrolyzed hydrochar presents a greater CO_2 sorption capacity (equal to 35 mg/g, corresponding to 0.79 mmol/g), owing to the pyrolysis treatment that has increased, to a limited extent, both the available surface and the volume of micropores, as previously stated. However, such CO_2 uptake is indicative of still unsatisfactory adsorption properties, which can be further improved. In this context, Pang et al. (2021), reported only mild CO_2 uptake, by testing biochar obtained after direct pyrolysis of hazelnut shells (CO_2 uptake = 1.56 mmol/g at 25 °C and 1 bar, for the best AC, having SSA = 93 m^2/g, V_P = 0.10 cm^3/g, and V_{MICRO} = 0.16 cm^3/g), thus confirming the need to perform a further chemical activation of the pyrolyzed carbonaceous material. In our case, activation with KOH and H_3PO_4 has led to ACs with higher sorption capacities, due to the further increase of microporosities (A_{mic} > 700 m^2/g as reported in Table 2). The comparison between the ACs obtained from the raw feedstocks showed that the best CO_2 uptakes were achieved for the raw biomass - KOH AC, which showed a lower MP-SSA and total microporosity than that of the raw biomass - H_3PO_4 AC, but narrower micropores (Table 2 and Supplementary material). This result suggests that CO_2 adsorption is favored by the strong adsorption potentials of narrow micropores toward CO_2 molecules enhancing pore filling, in agreement with Sevilla and Fuertes (2011a). Such a microporosity development after direct chemical activation of hazelnut shells has been previously proposed by Lewicka (2017), who claimed a very high CO_2 uptake (up to about 5 mmol/g at 25 °C, for the best AC, having SSA = 1963 m^2/g, V_P = 1.15 cm^3/g, and V_{MICRO} = 0.64 cm^3/g). Regarding the ACs synthesized from the pyrolyzed hydrochar, that activated by KOH treatment gave the highest adsorption capacity, with a maximum CO_2 uptake of about 90 mg/g (corresponding to 2.05 mmol/g), which can be certainly considered as a good performance if compared with those achieved with many commercial and lab-made adsorbents (Goel et al., 2021). As a comparison, CO_2 adsorption data for ACs obtained from a two-step activation procedure on the raw biomass, e.g. via pyrolysis of the hazelnut shells and cascade KOH activation of the corresponding biochar, have been reported only by Pang et al. (2021), by interposing an intermediate addition of melamine as N-doping component, for improving the AC basicity. The best-achieved CO_2 uptake was 4.23 mmol/g (186.2 mg/g) at 25 °C and 1 bar (SSA = 1696 m^2/g, V_P = 0.70 cm^3/g, and V_{MICRO} = 0.78 cm^3/g),

mainly attributable to the modification of the alkaline properties of the char, besides the development of microporosity. Considering other available data of very performing ACs towards CO_2 adsorption, Sreńscek-Nazzal and Kiełbasa (2019) have chemically modified commercial ACs by KOH treatment, obtaining the maximum CO_2 uptake of 3.67 mmol/g (161.5 mg/g) at 25 °C and 1 bar, and finely setting the optimal diameter range for CO_2 adsorption between 0.3 and 0.8 nm. Remarkably, our maximum CO_2 uptake is similar to those of ACs directly synthesized from similar waste biomasses, such as coconut shells (2.0 mmol/g, 88.0 mg/g) (Himeno et al., 2005) and almond shells (2.7 mmol/g, 118.8 mg/g) (Plaza et al., 2010). In this context, a high CO_2 uptake (4.2 mmol/g, 184.8 mg/g at 25 °C and 1 bar) was reported by Yang et al. (2017), after having optimized the KOH activation of coconut shells (SSA = 1963 m^2/g, V_P = 1.15 cm^3/g, and V_{MICRO} = 0.64 cm^3/g). Remarkably, the highest CO_2 uptake, amounting to 9.09 mmol/g (400 mg/g), was achieved by Toprak and Kopac (2017), but only for a specific type of KOH - AC (SSA = 2599 m^2/g, V_P = 1.16 cm^3/g, and V_{MICRO} = 1.04 cm^3/g), synthesized starting from a local coal. Anyway, the authors highlighted the exceptionality of this result, which may be due to the intrinsic properties of the starting coal.

Based on the above discussion, the available data on CO_2 uptakes of ACs are rather heterogeneous, differing for the precursors and the types of treatments that these have undergone, but CO_2 uptakes in the range of 2–4 mmol/g (88–176 mg/g) are certainly indicative of good adsorption properties. To further improve such adsorption performances, all the upstream treatments required for the AC synthesis, including both the carbonization treatment and the activation steps (type, number of steps, and operating conditions), should be carefully optimized. The aim should be the production of AC, as the main target product, characterized by finely tuned properties, based on the specific probe molecule to be adsorbed on. To achieve this primary goal, it would be necessary to optimize not only the downstream activation treatment(s) but also the upstream ones (carbonization step), in our case already aimed at the production of LA as the main product. Our maximum CO_2 uptake acquires a greater relevance, also after having considered that the starting hydrochar precursor is a waste of an already existing process, actually aimed at the production of a different marketable product (LA). Furthermore, our maximum CO_2 uptake has been obtained at more representative flue gas conditions (CO_2 partial pressure of 0.60 bar), evidencing the potential use of such AC for post-combustion CO_2 capture.

Based on the best-achieved results, pyrolyzed hydrochar - KOH AC was subjected to continuous cycles of CO_2 adsorption/desorption, to evaluate its potential regenerability. This property is economically impacting when the AC is used in filtration processes (Sevilla et al., 2012). CO_2 adsorption/desorption cycles for the pyrolyzed hydrochar - KOH AC have been carried out (Supplementary material), highlighting the excellent regenerability of the pyrolyzed hydrochar - KOH AC, even after 50 adsorption/desorption cycles. Moreover, it is remarkable that the equilibrium time, e.g. the time required to reach the maximum CO_2 adsorption, is very short (<10 min.).

3.4. Solid/liquid adsorption of MB

Raw biomass - H_3PO_4 AC and pyrolyzed hydrochar - KOH AC have been preliminarily tested for the removal of MB from aqueous solutions. MB is a well-known dye, and of particular interest for the wastewaters of the textile industry (Pandey et al., 2022). This molecule is accessible to adsorbents with pores>1.5 nm, e.g. with prevailing mesopores, given its average dimensions in the water medium (16.32 Å×5.64 Å×5.41 Å). A preliminary kinetic investigation was carried out on the raw hydrochar, to get information on its native adsorbing capacity. Experimental data (see Supplementary material) show that MB adsorption on the raw hydrochar is well-described by a pseudo-second-order model (k_2 = 1.00 g/mg·min; $q_{e, cal}$ = 0.18 mg/g vs $q_{e, exp}$ = 0.17 mg/g; R^2 = 0.9848). q_t data show that the adsorption capacity of the raw hydrochar is very low,

Table 3

MB adsorbed (in mg/g) and corresponding MB removal efficiency ($\eta\%$).

Test	AC/MB weight ratio	MB adsorbed on raw biomass - H_3PO_4 AC (mg/g)	η %	MB adsorbed on pyrolyzed hydrochar - KOH AC (mg/g)	η %
1	40	25.0	99.9	25.0	100.0
2	4	247.9	99.2	249.9	99.9

achieving the maximum amount of MB adsorbed per gram of adsorbent at the equilibrium (q_e) within 20 min. This represents the blank experiment for evaluating the effectiveness of ACs for removing MB from aqueous solutions. For the MB adsorption experiments on ACs, according to Paraskeva et al. (2008), a long contact time (17 h), neutral pH of the solution, and starting concentration of MB of 0.1 g/L have been chosen and kept constant, whilst only the AC/MB weight ratio was varied. The long contact time was chosen to guarantee the achievement of the equilibrium state, while the neutral pH minimizes possible charge modifications of the functional groups. On this basis, two preliminary adsorption tests have been performed, and the obtained results are reported in Table 3.

The above data highlight the good efficiency of the synthesized ACs towards MB removal. MB adsorption is favored by the prevailing mesoporosity of the raw biomass - H_3PO_4 AC (Table 2), as expected, because of its molecular dimensions. Remarkably, its removal is complete also in the case of the pyrolyzed hydrochar - KOH AC, despite its prevailing microporosities (Table 2). This observation can be justified considering that MB adsorption involves the external surface (rather than that internal, of greater interest for micropores), and it is further favored by the presence of its surface functional groups. The positive role of microporosity in improving MB adsorption is in agreement with evidence reported by Benadjemia et al. (2011), whereas such improvement was obtained up to a minimum diameter of 1.33 nm. The best experimental data reported in Table 3 were further verified for lower contact times, up to a minimum of 1 h. The highest amount of adsorbed MB per gram of adsorbent is good if compared with other available low-cost mesoporous ACs. Aygün et al. (2003) synthesized ACs by $ZnCl_2$ chemical activation of different waste biomasses, such as fruit stones and nutshells (hazelnut shells, apricot stones, walnut shells, and almond shells). Low MB adsorption capacities were reported for the corresponding ACs from shells (e.g. 8.82 mg/g of MB, for the best AC from hazelnut shells, having SSA = 793 m^2/g). Açıkyıldız et al. (2014) synthesized mesoporous ACs by $ZnCl_2$ activation of plant wastes (pine sawdust, rose seed, and cornel seed). The best ACs showed high SSAs (about 1000 m^2/g) and MB adsorption capacities close to 300 mg/g. Rattan (*Lacosperma secundiflorum*) wastes were hydrothermally carbonized and NaOH-activated by Islam et al. (2017), claiming good performances for MB removal (MB adsorption capacity = 359 mg/g, SSA = 1135 m^2/g, V_P = 0.61 cm^3/g, V_{MESO} = 0.44 cm^3/g). Remarkably, similar performances were reported by Lin et al. (2013), for the ACs synthesized starting from rice husk or hull, by a two-step activation procedure (pre-carbonization and NaOH activation), achieving a successful MB removal (MB adsorption capacity = 390 mg/g, for the best AC from rice waste, having SSA = 1015 m^2/g, V_P = 0.75 cm^3/g, V_{MESO} = 0.75 cm^3/g).

Based on the above comparative discussion, our pyrolyzed hydrochar - KOH AC has certainly good performance for MB adsorption, fully meeting the minimum standard criteria for MB adsorption, identified at 120 mg/g (Zulkania et al., 2018). An overall evaluation of the available MB adsorption data for such carbon materials, as deeply proposed by Santoso et al. (2020), confirms the judgment of moderate MB adsorption efficiency for our best AC. These preliminary data require further investigation but, at the current level of investigation, open the way to the use of the pyrolyzed hydrochar - KOH AC, for example for the removal of dyes from the wastewater of the textile industry.

In conclusion, our proposed three-step approach expands the hydrochar exploitation possibilities beyond its immediate energetic use, this latter is already recognized in net environmental savings (e.g. negative impact) (Berge et al., 2015). Further hydrochar environmental benefits will depend on the choice of the starting feedstock and final applications of the hydrochar-based products, taking into account possible economic and social benefits, often underestimated. In this context, hazelnut shells do not compete with the food chain, thus conceptually supporting the proposed cascade thermochemical approach. The progressive increase of carbon stability as a consequence of the proposed cascade approach, is a key aspect to achieve for the development of environmental applications of hydrochar. Moreover, the synthesis of ACs well fits within this context, also taking into account the very high added-value of such products. In addition, the proposed intermediate post-pyrolysis treatment allows for broadening the hydrochar exploitation possibilities, e.g. as an amendment or for soil remediation purposes. At this state of the art, the highlighted multifunctionality of the hydrochar well supports the circular bioeconomy concept, favorably reducing greenhouse gas emissions (Mak et al., 2020), and resulting well-integrable within the already existing LA production chain. However, further specific and integrated LCA evaluations are necessary to consider the real environmental impacts of hydrochar, which require much more experimental data and evaluations from an industrial perspective.

4. Conclusions

New activated carbons have been synthesized starting from the hydrochar recovered as the main waste stream, after the levulinic acid synthesis. For this purpose, a pyrolysis post-treatment of the hydrochar, followed by chemical activation treatments, have been evaluated, overall resulting in a three-step activation procedure. Chemical activation procedures have been replied on the starting biomass, to evaluate the change of the surface properties. Remarkably, H_3PO_4 activation should be advantageously proposed to produce mesoporous activated carbons from the raw biomass, whilst KOH is highly required for the prevailing development of microporosities starting from the pyrolyzed hydrochar. Both these activated carbons have been recovered in good yield (~78 wt% and ~ 65 wt%, respectively, evaluated with respect to the weight of the starting precursor), showing good surface properties. However, direct H_3PO_4 activation of the raw biomass does not allow the optimal exploitation of the cellulose fraction, while our proposed three-step approach, providing the KOH activation of the pyrolyzed hydrochar, fully satisfies this request, resulting well-placed within the existing production process of this platform chemical. Both carbon dioxide and methylene blue adsorption tests have highlighted the good performances of the pyrolyzed hydrochar - KOH activated carbon, given by a good synergy between micro- and meso-pores (Specific Surface Area: 1421 m^2/g, V_P: 0,63 cm^3/g, V_{MESO}: 0.10 cm^3/g, V_{MICRO}: 0.52 cm^3/g), opening the way to the possible exploitation of this hydrochar for new environmental applications.

Declaration of Competing Interest

The authors declare that they have no known competing financial interests or personal relationships that could have appeared to influence the work reported in this paper.

Data availability

The data that has been used is confidential.

Appendix A. Supplementary data

Supplementary data to this article can be found online at https://doi.org/10.1016/j.wasman.2023.06.012.

References

Açıkyıldız, M., Gürses, A., Karaca, S., 2014. Preparation and characterization of activated carbon from plant wastes with chemical activation. Micropor. Mesopor. Mat. 198, 45–49. https://doi.org/10.1016/j.micromeso.2014.07.018.

Alcañiz-Monge, J., Román-Martínez, M.D.C., Lillo-Ródenas, M.Á., 2022. Chemical activation of lignocellulosic precursors and residues: What else to consider? Molecules 27, 1630. https://doi.org/10.3390/molecules27051630.

Aygün, A., Yenisoy-Karakaş, S., Duman, I., 2003. Production of granular activated carbon from fruit stones and nutshells and evaluation of their physical, chemical and adsorption properties. Micropor. Mesopor. Mat. 66, 189–195. https://doi.org/10.1016/j.micromeso.2003.08.028.

Bahcivanji, L., Gascó, G., Paz-Ferreiro, J., Méndez, A., 2020. The effect of post-pyrolysis treatment on waste biomass derived hydrochar. Waste Manage. 106, 55–61. https://doi.org/10.1016/j.wasman.2020.03.007.

Benadjemia, M., Millière, L., Reinert, L., Benderdouche, N., Duclaux, L., 2011. Preparation, characterization and methylene blue adsorption of phosphoric acid activated carbons from globe artichoke leaves. Fuel Process. Technol. 92, 1203–1212. https://doi.org/10.1016/j.fuproc.2011.01.014.

Berge, N.D., Li, L., Flora, J.R.V., Ro, K.S., 2015. Assessing the environmental impact of energy production from hydrochar generated via hydrothermal carbonization of food wastes. Waste Manage. 43, 203–217. https://doi.org/10.1016/j.wasman.2015.04.029.

Björnerbäck, F., Hedin, N., 2019. Microporous humins prepared from sugars and bio-based polymers in concentrated sulfuric acid. ACS Sustain. Chem. Eng. 7, 1018–1027. https://doi.org/10.1021/acssuschemeng.8b04658.

Chaparro-Garnica, J., Guiton, M., Salinas-Torres, D., Morallón, E., Benetto, E., Cazorla-Amorós, D., 2022. Life cycle assessment of biorefinery technology producing activated carbon and levulinic acid. J. Clean. Prod. 380, 135098 https://doi.org/10.1016/j.jclepro.2022.135098.

Chen, L.Z., Miao, D.X., Feng, X.J., Xu, J.Z., 2014. Preparation and characterization of activated carbon from reedy grass leaves by chemical activation with KOH. Adv. Mater. Res. 881–883, 579–583. https://doi.org/10.4028/www.scientific.net/AMR.881-883.579.

Cheng, Z., Goulas, K.A., Rodriguez, N.Q., Saha, B., Vlachos, D.G., 2020. Growth kinetics of humins studied via X-ray scattering. Green Chem. 22, 2301–2309. https://doi.org/10.1039/C9GC03961A.

Correa, C.R., Stollovsky, M., Hehr, T., Rauscher, Y., Rolli, B., Kruse, A., 2017. Influence of the carbonization process on activated carbon properties from lignin and lignin-rich biomasses. ACS Sustain. Chem. Eng. 5, 8222–8233. https://doi.org/10.1021/acssuschemeng.7b01895.

Cui, X., Wang, J., Wang, X., Du, G., Khan, K.Y., Yan, B., Cheng, Z., Chen, G., 2022. Pyrolysis of exhausted hydrochar sorbent for cadmium separation and biochar regeneration. Chemosphere 306, 135546. https://doi.org/10.1016/j.chemosphere.2022.135546.

Delgado, C.N., Mendez, J.R.R., 2014. Preparation of carbon materials from lignocellulosic biomass. In: Rufford, T.E., Hulicova-Jurcakova, D., Zhu, J. (Eds.), Green Carbon Materials: Advances and Applications. Taylor & Francis Group, Boca Raton, pp. 35–64.

Deng, C., Lin, R., Kang, X., Wu, B., Ning, X., Wall, D., Murphy, J.D., 2022. Co-production of hydrochar, levulinic acid and value-added chemicals by microwave-assisted hydrothermal carbonization of seaweed. Chem. Eng. J. 441, 135915 https://doi.org/10.1016/j.cej.2022.135915.

Di Bucchianico, D.D.M., Wang, Y., Buvat, J.-C., Pan, Y., Moreno, V.C., Leveneur, S., 2022. Production of levulinic acid and alkyl levulinates: a process insight. Green Chem. 24, 614–646. https://doi.org/10.1039/D1GC02457D.

Dutta, S., Zhang, Q., Cao, Y., Wu, C., Moustakas, K., Zhang, S., Wong, K.-H., Tsang, D.C.W., 2022a. Catalytic valorisation of various paper wastes into levulinic acid, hydroxymethylfurfural, and furfural: Influence of feedstock properties and ferric chloride. Bioresour. Technol. 357, 127376 https://doi.org/10.1016/j.biortech.2022.127376.

Dutta, S., Yu, I.K.M., Fan, J., Clark, J.H., Tsang, D.C.W., 2022b. Critical factors for levulinic acid production from starch-rich food waste: solvent effects, reaction

pressure, and phase separation. Green Chem. 24, 163–175. https://doi.org/10.1039/D1GC01948A.

Falco, C., Caballero, F.P., Babonneau, F., Gervais, C., Laurent, G., Titirici, M.-M., Baccile, N., 2011. Hydrothermal carbon from biomass: structural differences between hydrothermal and pyrolyzed carbons via ^{13}C solid state NMR. Langmuir 27, 14460–14471. https://doi.org/10.1021/la202361p.

Gao, Y., Yue, Q., Gao, B., Li, A., 2020. Insight into activated carbon from different kinds of chemical activating agents: A review. Sci. Total Environ. 746, 141094 https://doi.org/10.1016/j.scitotenv.2020.141094.

Gascó, G., Paz-Ferreiro, J., Álvarez, M.L., Saa, A., Méndez, A., 2018. Biochars and hydrochars prepared by pyrolysis and hydrothermal carbonisation of pig manure. Waste Manage. 79, 395–403. https://doi.org/10.1016/j.wasman.2018.08.015.

http://www.gfbiochemicals.com/technology/ (accessed 14-03-2023).

Goel, C., Mohan, S., Dinesha, P., 2021. CO_2 capture by adsorption on biomass-derived activated char: A review. Sci. Total Environ. 798, 149296 https://doi.org/10.1016/j.scitotenv.2021.149296.

Güleç, F., Williams, O., Kostas, E.T., Samson, A., Stevens, L.A., Lester, E., 2022. A comprehensive comparative study on methylene blue removal from aqueous solution using biochars produced from rapeseed, whitewood, and seaweed via different thermal conversion technologies. Fuel 330, 125428. https://doi.org/10.1016/j.fuel.2022.125428.

He, M., Zhu, X., Dutta, S., Khanal, S.K., Lee, K.T., Masek, O., Tsang, D.C.W., 2022. Catalytic co-hydrothermal carbonization of food waste digestate and yard waste for energy application and nutrient recovery. Bioresour. Technol. 344, 126395 https://doi.org/10.1016/j.biortech.2021.126395.

Himeno, S., Komatsu, T., Fujita, S., 2005. High-pressure adsorption equilibria of methane and carbon dioxide on several activated carbons. J. Chem. Eng. Data 50, 369–376. https://doi.org/10.1021/je049786x.

Hurtado, S.I.M., Puello, P., Cabarcas, A., 2021. Technical evaluation of a levulinic acid plant based on biomass transformation under techno-economic and exergy analyses. ACS Omega 6, 5627–5641. https://doi.org/10.1021/acsomega.0c06088.

Islam, M.A., Ahmed, M.J., Khanday, W.A., Asif, M., Hameed, B.H., 2017. Mesoporous activated carbon prepared from NaOH activation of rattan (Lacosperma secundiflorum) hydrochar for methylene blue removal. Ecotoxicol. Environ. Saf. 138, 279–285. https://doi.org/10.1016/j.ecoenv.2017.01.010.

Jibril, B., Houache, O., Al-Maamari, R., Al-Rashidi, B., 2008. Effects of H_3PO_4 and KOH in carbonization of lignocellulosic material. J. Anal. Appl. Pyrolysis 83, 151–156. https://doi.org/10.1016/j.jaap.2008.07.003.

Kabakcı, S.B., Baran, S.S., 2019. Hydrothermal carbonization of various lignocellulosics: Fuel characteristics of hydrochars and surface characteristics of activated hydrochars. Waste Manage. 100, 259–268. https://doi.org/10.1016/j.wasman.2019.09.021.

Kumar, A., Saini, K., Bhaskar, T., 2020. Hydrochar and biochar: Production, physicochemical properties and technoeconomic analysis. Bioresour. Technol. 310, 123442 https://doi.org/10.1016/j.biortech.2020.123442.

Lewicka, K., 2017. Activated carbons prepared from hazelnut shells, walnut shells and peanut shells for high CO_2 adsorption. Polish J. Chem. Technol. 19, 38–43. https://doi.org/10.1515/pjct-2017-0025.

Libra, J.A., Ro, K.S., Kammann, C., Funke, A., Berge, N.D., Neubauer, Y., Titirici, M.-M., 2011. Hydrothermal carbonization of biomass residuals: A comparative review of the chemistry, processes and applications of wet and dry pyrolysis. Biofuels 2, 89–124. https://doi.org/10.4155/bfs.10.81.

Licursi, D., Antonetti, C., Fulignati, S., Vitolo, S., Puccini, M., Ribechini, E., Bernazzani, L., Raspolli Galletti, A.M., 2017. In-depth characterization of valuable char obtained from hydrothermal conversion of hazelnut shells to levulinic acid. Bioresour. Technol. 244, 880–888. https://doi.org/10.1016/j.biortech.2017.08.012.

Lin, L., Zhai, S.-R., Xiao, Z.-Y., Song, Y., An, Q.-D., Song, X.-W., 2013. Dye adsorption of mesoporous activated carbons produced from NaOH-pretreated rice husks. Bioresour. Technol. 136, 437–443. https://doi.org/10.1016/j.biortech.2013.03.048.

Liu, H., Chen, Y., Yang, H., Gentili, F.G., Söderlind, U., Wang, X., Zhang, W., Chen, H., 2019. Hydrothermal carbonization of natural microalgae containing a high ash content. Fuel 249, 441–448. https://doi.org/10.1016/j.fuel.2019.03.004.

Mak, T.M.W., Xiong, X., Tsang, D.C.W., Yu, I.K.M., Poon, C.S., 2020. Sustainable food waste management towards circular bioeconomy: Policy review, limitations and opportunities. Bioresour. Technol. 297, 122497 https://doi.org/10.1016/j.biortech.2019.122497.

Molina-Sabio, M., Rodrìguez-Reinoso, F., 2004. Role of chemical activation in the development of carbon porosity. Colloids Surf. A 241, 15–25. https://doi.org/10.1016/j.colsurfa.2004.04.007.

Pandey, D., Daverey, A., Dutta, K., Yata, V.K., Arunachalam, K., 2022. Valorization of waste pine needle biomass into biosorbents for the removal of methylene blue dye from water: Kinetics, equilibrium and thermodynamics study. Environ. Technol. Innov. 25, 102200 https://doi.org/10.1016/j.eti.2021.102200.

Pang, R., Lu, T., Shao, J., Wang, L., Wu, X., Qian, X., Hu, X., 2021. Highly efficient nitrogen-doped porous carbonaceous CO_2 adsorbents derived from biomass. Energy Fuels 35, 1620–1628. https://doi.org/10.1021/acs.energyfuels.0c03832.

Paraskeva, P., Kalderis, D., Diamadopoulos, E., 2008. Production of activated carbon from agricultural by-products. J. Chem. Technol. Biotechnol. 83, 581–592. https://doi.org/10.1002/jctb.1847.

Plaza, M.G., Pevida, C., Martin, C.F., Fermoso, J., Pis, J.J., Rubiera, F., 2010. Developing almond shell-derived activated carbons as CO_2 adsorbents. Sep. Purif. Technol. 71, 102–106. https://doi.org/10.1016/j.seppur.2009.11.008.

Rao Ganga, V.S., Dabbawala, A.A., Munusamy, K., Abdi, S.H.R., Kureshy, R.I., Khan, N.H., Bajaj, H.C., 2016. Rhodium complexes supported on nanoporous activated carbon for selective hydroformylation of olefins. Catal. Commun. 84, 21–24. https://doi.org/10.1016/j.catcom.2016.05.021.

Rechnia, P., Malaika, A., Najder-Kozdrowska, L., Kozlowski, M., 2012. The effect of ethanol on carbon-catalysed decomposition of methane. Int. J. Hydrog. Energy 37, 7512–7520. https://doi.org/10.1016/j.ijhydene.2012.02.014.

Rivas, S., Moure, A., Parajó, J.C., 2020. Pretreatment of hazelnut shells as a key strategy for the solubilization and valorization of hemicelluloses into bioactive compounds. Agronomy 10, 760. https://doi.org/10.3390/agronomy10060760.

Romero-Anaya, A.J., Ouzzine, M., Lillo-Ródenas, M.A., Linares-Solano, A., 2014. Spherical carbons: Synthesis, characterization and activation processes. Carbon 68, 296–307. https://doi.org/10.1016/j.carbon.2013.11.006.

Sajjadi, B., Chen, W.-Y., Egiebor, N.O., 2018. A comprehensive review on physical activation of biochar for energy and environmental applications. Rev. Chem. Eng. 35 https://doi.org/10.1515/revce-2017-0113.

Santana Junior, C.C., Brito, M.R., Barbosa, L.N., Jaconi, A., Rambo, M.K.D., Rambo, M.C. D., 2020. Environmental-economic assessment of lignocellulosic residual from the Legal Amazon for conversion in biochars and bioproducts for biorefineries. Int. J. Adv. Eng. Res. Sci. 7, 324–337. https://doi.org/10.22161/ijaers.78.36.

Santoso, E., Ediati, R., Kusumawati, Y., Bahruji, H., Sulistiono, D.O., Prasetyoko, D., 2020. Review on recent advances of carbon based adsorbent for methylene blue removal from waste water. Mater. Today Chem. 16, 100233 https://doi.org/10.1016/j.mtchem.2019.100233.

Sevilla, M., Ferrero, G.A., Fuertes, A.B., 2019. CO₂ storage on nanoporous carbons. In: Kaneko, K., Rodríguez-Reinoso, F. (Eds.), Nanoporous materials for gas storage, green energy and technology. Springer Nature Singapore Pte Ltd, Singapore, pp. 287–330.

Sevilla, M., Falco, C., Titirici, M.-M., Fuertes, A.B., 2012. High-performance CO₂ sorbents from algae. RSC Adv. 2, 12792–12797. https://doi.org/10.1039/C2RA22552B.

Sevilla, M., Fuertes, A.B., 2011a. Sustainable porous carbons with a superior performance for CO₂ capture. Energy Environ. Sci. 4, 1765–1771. https://doi.org/10.1039/C0EE00784F.

Sevilla, M., Fuertes, A.B., Mokaya, R., 2011b. High density hydrogen storage in superactivated carbons from hydrothermally carbonized renewable organic materials. Energy Environ. Sci. 4, 1400–1410. https://doi.org/10.1039/C0EE00347F.

Shi, N., Liu, Q., He, X., Wang, G., Chen, N., Peng, J., Ma, L., 2019. Molecular structure and formation mechanism of hydrochar from hydrothermal carbonization of carbohydrates. Energy Fuels 33, 9904–9915. https://doi.org/10.1021/acs.energyfuels.9b02174.

Shinde, S.D., Meng, X., Kumar, R., Ragauskas, A.J., 2018. Recent advances in understanding the pseudo-lignin formation in a lignocellulosic biorefinery. Green Chem. 20, 2192–2205. https://doi.org/10.1039/C8GC00353J.

Sreńscek-Nazzal, J., Kiełbasa, K., 2019. Advances in modification of commercial activated carbon for enhancement of CO₂ capture. Appl. Surf. Sci. 494 (15), 137–151. https://doi.org/10.1016/j.apsusc.2019.07.108.

https://www.statista.com/statistics/1030790/tree-nut-global-production-by-type/ (accessed 25-05-2022).

Silva, J.F.L., Grekin, R., Mariano, A.P., Filho, R.M., 2018. Making levulinic acid and ethyl levulinate economically viable: a worldwide techno-economic and environmental assessment of possible routes. Energy Technol. 6, 613–639. https://doi.org/10.1002/ente.201700594.

Suárez-García, F., Martínez-Alonso, A., Tascón, J.M.D., 2002. Pyrolysis of apple pulp: chemical activation with phosphoric acid. J. Anal. Appl. Pyrolysis 63, 283–301. https://doi.org/10.1016/S0165-2370(01)00160-7.

Toprak, A., Kopac, T., 2017. Carbon dioxide adsorption using high surface area activated carbons from local coals modified by KOH, NaOH and ZnCl₂ agents. Int. J. Chem. React. 15, 20160042. https://doi.org/10.1515/ijcre-2016-0042.

Tran, H.N., You, S.-J., Chao, H.-P., 2017. Fast and efficient adsorption of methylene green 5 on activated carbon prepared from new chemical activation method. J. Environ. Manage. 188, 322–336. https://doi.org/10.1016/j.jenvman.2016.12.003.

Tripathi, M., Sahu, J.N., 2016. Effect of process parameters on production of biochar from biomass waste through pyrolysis: A review. Renew. Sust. Energ. Rev. 55, 467–481. https://doi.org/10.1016/j.rser.2015.10.122.

Unur, E., 2013. Functional nanoporous carbons from hydrothermally treated biomass for environmental purification. Microporous Mesoporous Mater. 168, 92–101. https://doi.org/10.1016/j.micromeso.2012.09.027.

van Zandvoort, I., van Eck, E.R.H., de Peinder, P., Heeres, H.J., Bruijnincx, P.C.A., Weckhuysen, B.W., 2015. Full, reactive solubilization of humin byproducts by alkaline treatment and characterization of the alkali-treated humins formed. ACS Sustain. Chem. Eng. 3, 533–543. https://doi.org/10.1021/sc500772w.

Wan, G., Zhang, Q., Li, M., Jia, Z., Guo, C., Luo, B., Wang, S., Min, D., 2019. How pseudo-lignin is generated during dilute sulfuric acid pretreatment. J. Agric. Food Chem. 67, 10116–10125. https://doi.org/10.1021/acs.jafc.9b02851.

Wang, X., Chi, Q., Liu, X., Wang, Y., 2019. Influence of pyrolysis temperature on characteristics and environmental risk of heavy metals in pyrolyzed biochar made from hydrothermally treated sewage sludge. Chemosphere 216, 698–706. https://doi.org/10.1016/j.chemosphere.2018.10.189.

Wang, L., Guo, Y., Zou, B., Rong, C., Ma, X., Qu, Y., Li, Y., Wang, Z., 2011. High surface area porous carbons prepared from hydrochars by phosphoric acid activation. Bioresour. Technol. 102, 1947–1950. https://doi.org/10.1016/j.biortech.2010.08.100.

Wortmann, M., Keil, W., Brockhagen, B., Biedinger, J., Westphal, M., Weinberger, C., Diestelhorst, E., Hachmann, W., Zhao, Y., Tiemann, M., Reiss, G., Hüsgen, B., Schmidt, C., Sattler, K., Frese, N., 2022. Pyrolysis of sucrose-derived hydrochar. J. Anal. Appl. Pyrolysis 161, 105404. https://doi.org/10.1016/j.jaap.2021.105404.

Xu, J., Chen, L., Qu, H., Jiao, Y., Xie, J., Xing, G., 2014. Preparation and characterization of activated carbon from reedy grass leaves by chemical activation with H₃PO₄. Appl. Surf. Sci. 320, 674–680. https://doi.org/10.1016/j.apsusc.2014.08.178.

Yang, J., Yue, L., Hu, X., Wang, L., Zhao, Y., Lin, Y., Sun, Y., DaCosta, H., Guo, L., 2017. Efficient CO₂ capture by porous carbons derived from coconut shell. Energy Fuels 31, 4287–4293. https://doi.org/10.1021/acs.energyfuels.7b00633.

Yue, L., Xia, Q., Wang, L., Wang, L., DaCosta, H., Yang, J., Hu, X., 2018. CO₂ adsorption at nitrogen-doped carbons prepared by K₂CO₃ activation of urea-modified coconut shell. J. Colloid Interface Sci. 511, 259–267. https://doi.org/10.1016/j.jcis.2017.09.040.

Zhang, X., Wang, Y., Cai, J., Wilson, K., Lee, A.F., 2020. Bio/hydrochar sorbents for environmental remediation. Energy Environ. Mater. 3, 453–468. https://doi.org/10.1002/eem2.12074.

Zubbri, N.A., Mohamed, A.R., Lahijani, P., Mohammadi, M., 2021. Low temperature CO₂ capture on biomass-derived KOH-activated hydrochar established through hydrothermal carbonization with water-soaking pre-treatment. J. Environ. Chem. Eng. 9, 105074 https://doi.org/10.1016/j.jece.2021.105074.

Zubrik, A., Matik, M., Hredzák, S., Lovás, M., Danková, Z., Kováčová, M., Briančin, J., 2017. Preparation of chemically activated carbon from waste biomass by single-stage and two-stage pyrolysis. J. Clean. Prod. 143, 643–653. https://doi.org/10.1016/j.jclepro.2016.12.061.

Zulkania, A., Hanum, F.G., Rezki, A.S., 2018. The potential of activated carbon derived from bio-char waste of bio-oil pyrolysis as adsorbent. MATEC Web of Conferences 154, 01029. https://doi.org/10.1051/matecconf/201815401029.